Sensors & Actuators: A. Physical 393 (2025) 116855

Contents lists available at ScienceDirect

Sensors and Actuators: A. Physical

journal homepage: www.journals.elsevier.com/sensors-and-actuators-a-physical

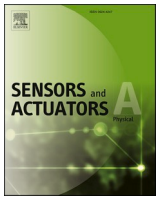

Miniature fiber optic pressure probe for inlet flow field measurements

Xi Chen [a,1], Zhengkang Lin [b,1], Fen Xiong [c], Hexia Huang [b,*], Ye Chen [c,*], Huijun Tan [b,*], Fei Xu [a,*]

[a] College of Engineering and Applied Sciences, Nanjing University, Nanjing 210023, China
[b] College of Energy and Power Engineering, Nanjing University of Aeronautics and Astronautics, Nanjing 210016, China
[c] College of Physics, MIIT Key Laboratory of Aerospace Information Materials and Physics, Nanjing University of Aeronautics and Astronautics, Nanjing 211106, China

ARTICLE INFO

Keywords:
Pressure measurements
Fiber-optic Fabry-Perot (FP) sensor
Miniature pressure probe
Inlet
High-speed flow field

ABSTRACT

Pressure monitoring of high-speed vehicles during ground and flight testing is critically important for aerodynamic characterization. In this study, we demonstrate a miniature optical pressure probe based on a 125-μm-diameter fiber-optic Fabry-Perot (FP) sensor for high-speed flow field measurements. The probe, with an ultracompact packaging size of 0.5 mm, was co-located with a commercial electrical probe for simultaneous testing in a subsonic flow field (Mach 0.29–0.61) at a 30 kHz sampling rate. Experimental results indicate that the optical probe achieves a resolution of 0.09 % F.S. (0–200 kPa) and a response delay of < 0.05 ms. Compared to electrical probes with similar performance specifications, the optical probe exhibits a significantly reduced footprint, while offering distinct advantages for high-speed, high-spatial-resolution, and high-accuracy flow field measurements.

1. Introduction

Advanced aircraft seek high stability, high performance, and enhanced aerodynamic efficiency. The inlet is crucial to sustaining the aero-engine's normal operation and enhancing the aircraft's performance; therefore, optimizing the inlet structure design and accurately assessing it during both ground and flight testing. The complex and transient character of the flow field, along with the growing complexity of inlet structures, impose increasing demands on the accuracy, response time, and spatial resolution of the measurements.

Various techniques have been developed for aerodynamic measurements of flow fields. Particle image velocimetry (PIV) [1] and laser Doppler velocimetry (LDV) [2] are two typical optical measurement techniques. PIV is better suited for assessing flow statistics like mean velocity than instantaneous fields [1], while LDV requires traversing a single-point probe to numerous flow locations, which makes it challenging to apply to measurements of unstable flow fields. Additionally, the application scenarios for both approaches are limited because they require optical access with transparent windows. Fast-response aerodynamic probes (FRAPs) have garnered increasing interest in aerospace testing due to their dependability, affordability, and user-friendliness [3]. State-of-the-art FRAPs are mainly based on electrical sensors, which can be divided into resistive, piezo-resistive, capacitive, and piezo-electric sensors [4,5]. Piezo-electric and piezo-resistive sensors are the primary options for measuring pressure because of their excellent accuracy and frequency responsiveness. Nevertheless, electrical sensors are susceptible to electromagnetic interference (EMI) and impose stringent requirements on environmental conditions such as temperature, humidity, and cleanliness during measurements. Furthermore, the minimum diameter of commercially available electrical sensors is around 1.5 mm, which does not allow for direct high spatial density alignment. To tackle this issue, current methods require the use of probe rakes to channel pressure through connecting conduits to back-end transducers in order to assess the fine spatial features of the flow field [6]. However, the long transmission distances through connecting conduits may lead to a long response time for the airflow, and the dynamic response may be impaired, which is detrimental to the measurement of dynamic aberrations [7]. In the meantime, internal fluid friction and wall friction of the lengthy connecting conduits will account for some of the energy loss because of viscous resistance, which directly results in low measurement accuracy and pressure loss. It is therefore imperative to develop new approaches that may simultaneously meet the needs of accuracy, speed, and spatial resolution while also being more resilient in challenging environments.

* Corresponding authors.
E-mail addresses: huanghexia@nuaa.edu.cn (H. Huang), yechen@nuaa.edu.cn (Y. Chen), tanhuijun@nuaa.edu.cn (H. Tan), feixu@nju.edu.cn (F. Xu).
[1] These authors contributed equally to this work as co-first authors.

https://doi.org/10.1016/j.sna.2025.116855
Received 28 April 2025; Received in revised form 20 June 2025; Accepted 30 June 2025
Available online 1 July 2025

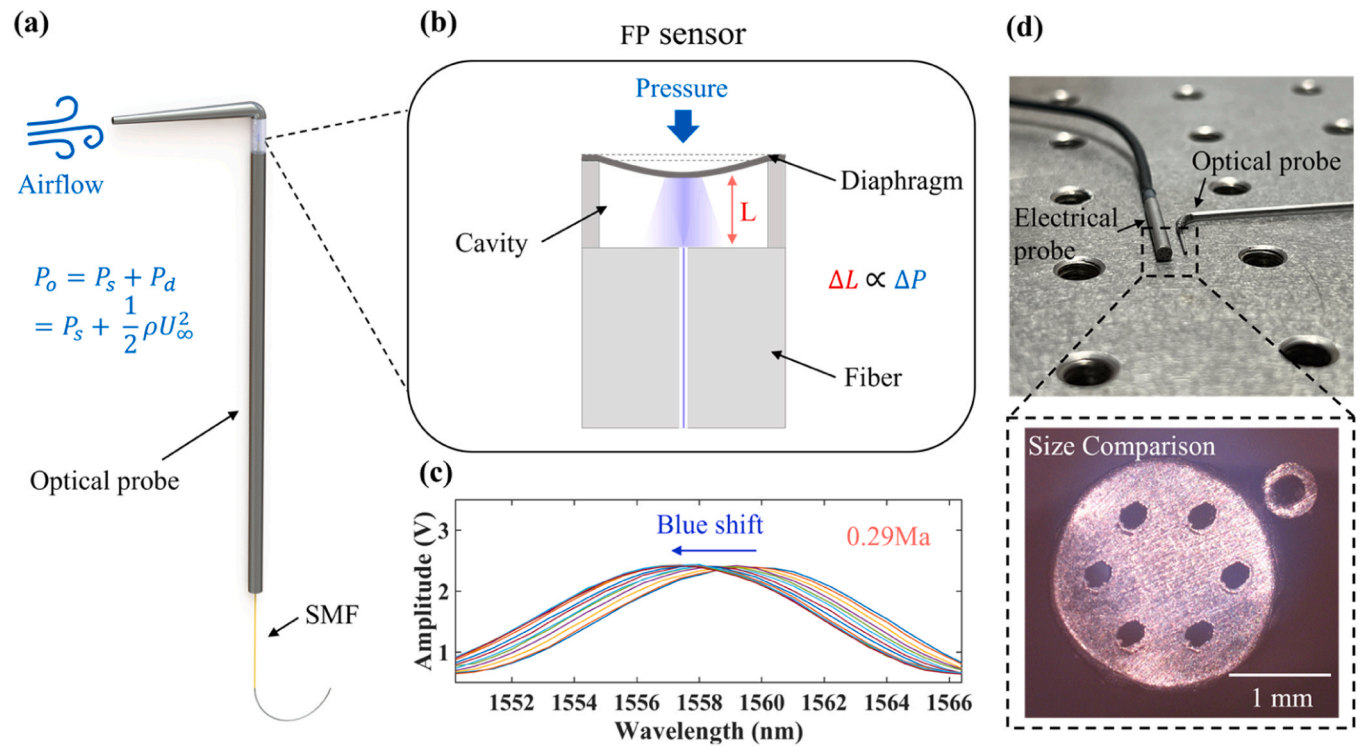

Fig. 1. Configuration of the proposed sensor, (a) the working principle and the structure of the FP sensor-integrated optical pressure probe, (b) schematic diagram of the working principle of a fiber-optic FP sensor, (c) the shift in the output interference spectra of the fiber-optic FP sensor at a Mach number of 0.29 Ma, (d) size comparison with a commercial small-size (2.2 mm) electrical probe and view under the microscope.

Because of its small size, high accuracy, and resistance to electromagnetic interference [8–12], fiber-optic Fabry-Perot (FP) sensor shows great potential for aerospace and aviation measurements in hash environment [13–15]. The fiber-optic Pitot-tube FP sensor plays a crucial role in high-speed gas flow measurement by directly acquiring the pressure difference between total pressure and static pressure [16,17]. Recent studies have reported all-glass miniature fiber-optic Pitot-tube sensor capable of in-situ flow velocity measurements in clean gas environments [18]. In other flow field measurement scenarios, fiber-optic FP sensor based FRAPs with varying materials and structural designs have been developed [19–24], such as all-silicon structure and metal diaphragm based FP sensor. Nevertheless, conventional all-silicon FP cavities demonstrate substantial device footprints, typically exhibiting 1–10 mm diameter/height dimensions [21–24], constrained by current microfabrication limitations. Furthermore, the structural integrity of the fiber-sensor interface limits their application in hash fluid measurement scenarios with confined spaces such as inlets. Sensors with reduced lateral dimensions enable enhanced spatial resolution, albeit at the expense of more stringent fabrication requirements—particularly regarding diaphragm thickness reduction to maintain adequate sensitivity and pressure resolution. Recent advances have demonstrated vector probe (Ø3 mm) integrating miniaturized fiber-optic FP pressure sensors incorporating metal diaphragms at 125 μm diameters [20]. Nevertheless, the predominant UV-adhesive-based packaging methodology [25,26] fundamentally constrains operational durability in hygroscopic or corrosive environments. This limitation is further exacerbated by significant nonlinearity (>15 % FS) in sensor response, which substantially hinders practical implementation. Consequently, developing FRAPs that simultaneously achieve miniaturization, environmental robustness, and high linearity (nonlinearity <1 % FS) remains an essential research challenge for extreme flow-field characterization.

In this study, we present a 0.5-mm-diameter optical pressure probe incorporating a miniaturized all-silica fiber-optic FP sensor (Ø125 μm) for high-speed flow field characterization. Owing to its ultracompact size, the FP sensor can be incorporated close to the port of the probe, thereby enhancing both measurement accuracy and temporal response - a critical advantage for unsteady flow measurements. Furthermore, the gold-coated all-silica FP sensing element eliminates adhesive bonding requirements, substantially improving the sensor's long-term stability and environments robustness under harsh operating conditions. The dynamic performance of the optical pressure probe was experimentally evaluated in a subsonic wind tunnel (Mach 0.29–0.61) at a 30 kHz sampling rate, with comparison to commercial silicon piezo-resistive probes. The results demonstrate that our optical probe exhibits superior responsiveness and detection accuracy compared to conventional piezoresistive counterparts. By combining ultraminiaturized design, high measurement fidelity, high-frequency sampling capability, exceptional stability, broad dynamic range, and electromagnetic interference immunity, the proposed optical pressure probe offers significant potential for high-spatial-resolution measurements in unsteady flow fields.

2. Design and principle

2.1. Structure of fiber optic sensor-integrated pressure probe

The working principle of a pressure probe relies on the stagnation of the flow around the probe. Stagnation occurs around the probes when probes are inserted into an inlet for a pressure field measurement. The pressure distribution around its tip can be described as a maximum pressure at the stagnant point and lower pressure at other points around it. Based on the conservation of energy, the total pressure P_0 at the measurement point can be expressed as the sum of the static and dynamic pressures P_s and P_d, neglecting mechanical losses,

$$P_o = P_s + P_d = P_s + \frac{1}{2}\rho U_\infty^2 \quad (1)$$

where U_∞ is the flow velocity, and ρ (kg/m^3) is the density of the fluid.

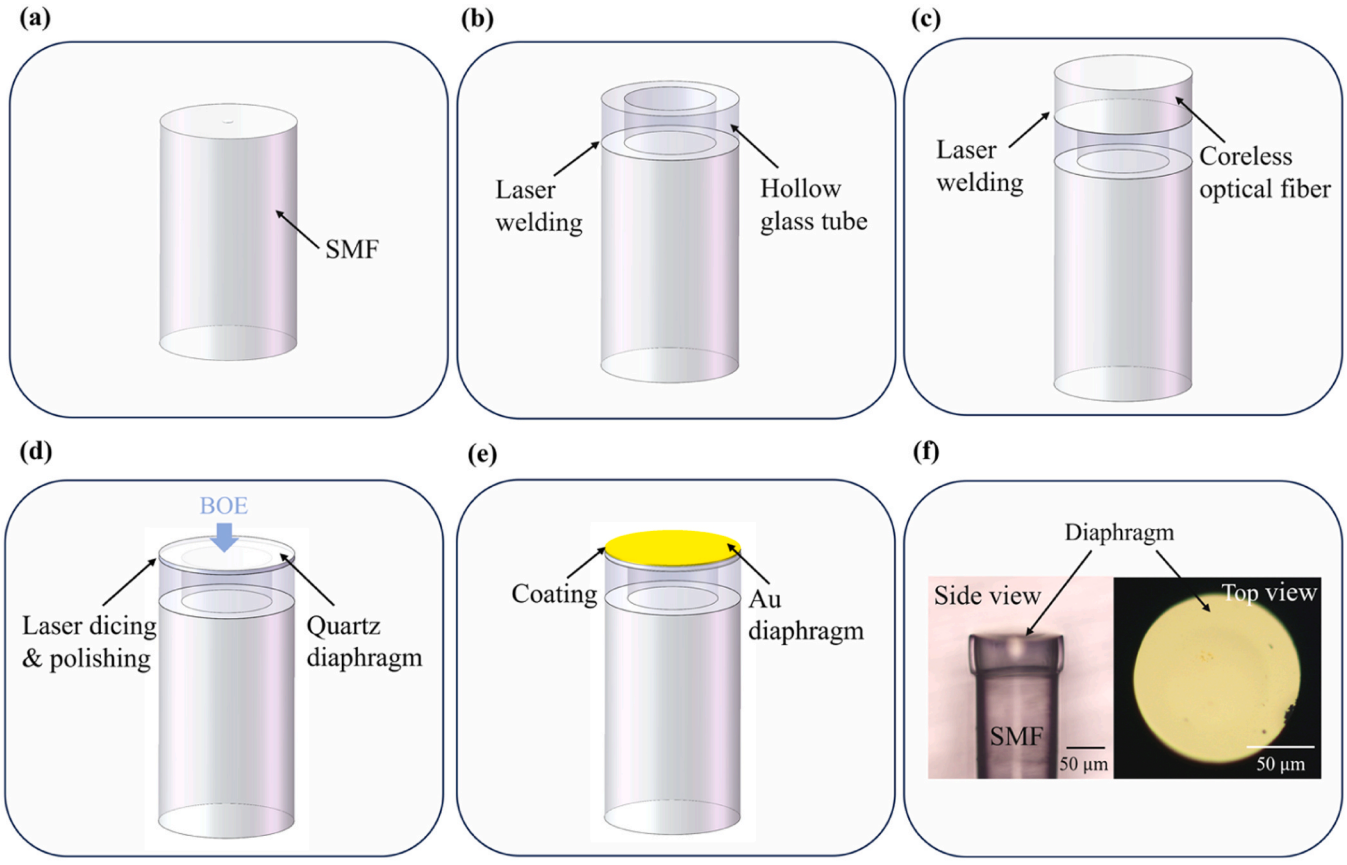

Fig. 2. Fabrication process of a typical FP pressure sensor, (a) SMF, (b) the hollow glass tube was fused to the SMF, (c) the CLF was fusion-bonded to the hollow glass tube, (d) grinding and polishing, (e) deposit gold film, (f) side and top views of the proposed fiber-optic FP sensor.

For the measurement of the steady state pressure field of the inlet, pressure probes are usually arranged on the AIP, and the port pressures derived from the probes are guided by conduits and then measured through the connection of back-end transducers. However, internal fluid friction and wall friction will cause some energy loss due to viscous drag during the long-distance transfer of airflow, and aerodynamic pressure loss can be obtained by estimation of the

$$P_{loss} = (\alpha \frac{l}{d}) \rho \frac{v^2}{2} \tag{2}$$

where P_{loss}, a, l, d, and v (m/s) are pressure loss, coefficient of frictional drag, length of the conduit, the inner diameter of the conduit, and velocity of the fluid, respectively. A large size of the probe's top area can result in excessive blockage ratios and perturbations to the flow field. However, the above method, such as dynamic aberration measurements, cannot be used for unsteady flow, where high-frequency time-varying pressure fluctuations can be attenuated during long-distance transmission.

Considering the aforementioned analysis, the FP sensor must be small enough to be installed near the probe's port in order to meet the requirements of unsteady flow measurements. The internal fiber-optic FP sensor and the external stainless steel casing that make up the main structure of the FP sensor-integrated pressure probe that we built are depicted in Fig. 1(a). The single-mode fiber (SMF) extending from the optical pressure probe is connected to self-developed high-speed demodulation system. Fig. 1(b) illustrates the working principle of the fiber-optic FP sensor. External pressure variations induce diaphragm deformation in the sensor, thereby modulating the optical path length (OPL), which ultimately leads to shifts in the interference spectrum. Here, Fig. 1(c) shows the blue shift of the sensor's interference spectrum at an incoming flow velocity of 0.29 Mach. The size of the fiber optic FP sensor is about 125 μm in diameter and 50 μm in length. Here, the diameter of the packaged probe is approximately 500 μm, and its comparison with the current typical commercial small-size (2.1 mm in diameter) electrical probe is shown in Fig. 1(d).

2.2. Design and fabrication of FP sensor in the probe

Based on the principle of the FP interferometer, the interference spectrum can be expressed as an intensity-modulated signal,

$$I = I_1 + I_2 + 2\sqrt{I_1 I_2}\cos(\frac{4\pi nL}{\lambda} + \pi) \tag{3}$$

where I represents the intensity of the interference spectrum, I_1 and I_2 are the intensities of the two reflections, n is the refractive index of the filling medium in the FP cavity, L is the length of the FP cavity, λ is the operating wavelength, and Π is the additional phase of the half-wave loss. It can be inferred that when the FP cavity length changes due to external influences, the interference spectrum also undergoes fluctuations. Methods including intensity demodulation [27,28], phase demodulation [29], the Fourier transform demodulation [30,31], correlation demodulation [32,33] and neural network demodulation [34,35] have been developed. The diaphragm thickness and cavity length parameters require a specific design that is in accordance with various demodulation methods and actual measurement requirements.

As illustrated in Fig. 1(b), when the sensor is exposed to external pressure, the central deformation of the sensing diaphragm L, i.e., the change in FP cavity length, can be expressed as

$$\Delta L = \frac{3(1-\gamma^2)a^4}{16Eh^3}\Delta P \tag{4}$$

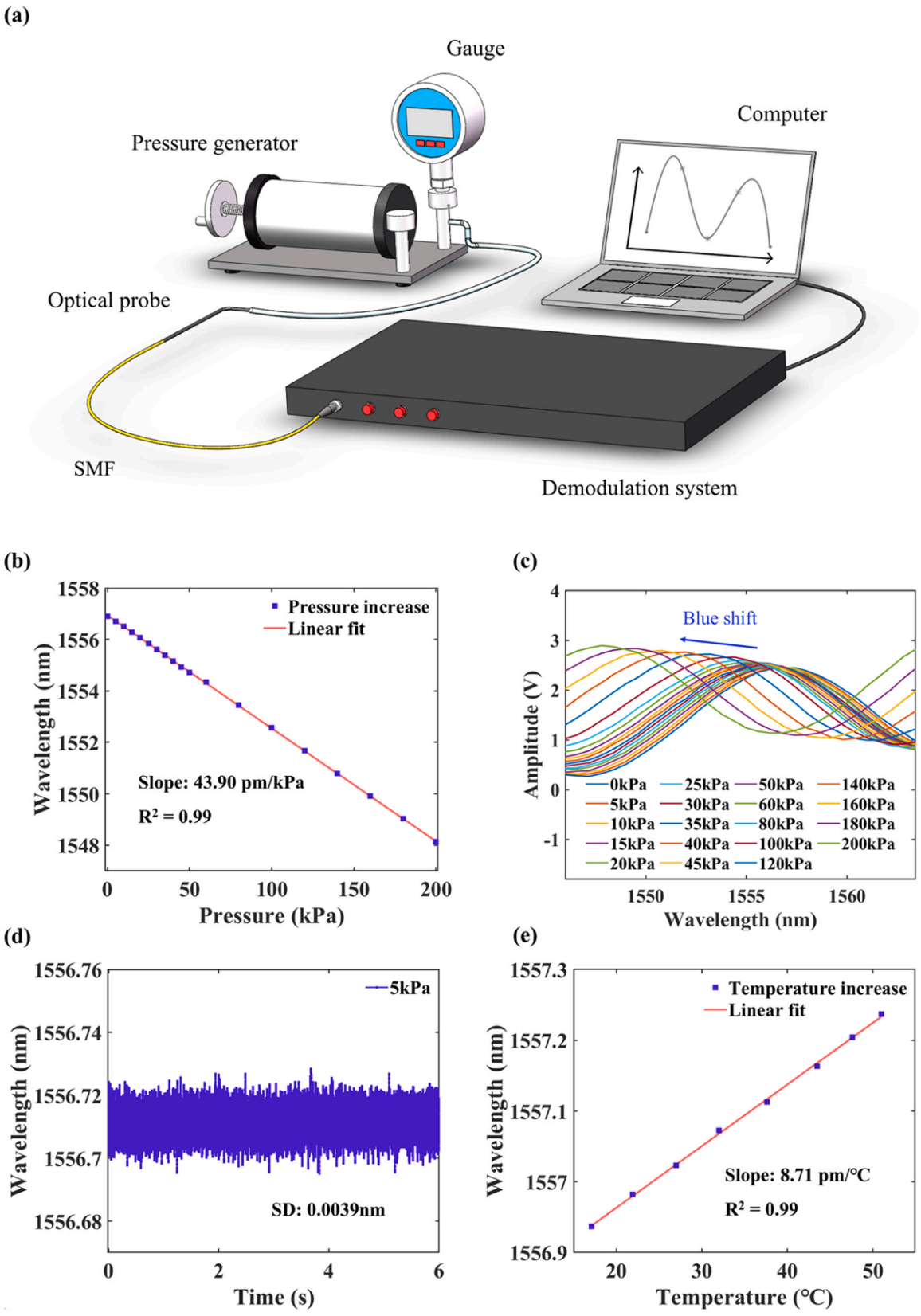

Fig. 3. Calibration of the FP sensor integrated pressure probes, (a) the experimental setup for the pressure tests, (b) the pressure response of the FP sensor in the range of 0~200 kPa, (c) the shift in the output interference spectra of the FP sensor in the range of 0~200 kPa, (d) the changes of the measured wavelength when the pressure is 5 kPa within 6 s, (e) the temperature response of the FP sensor in the range of 17–51 °C.

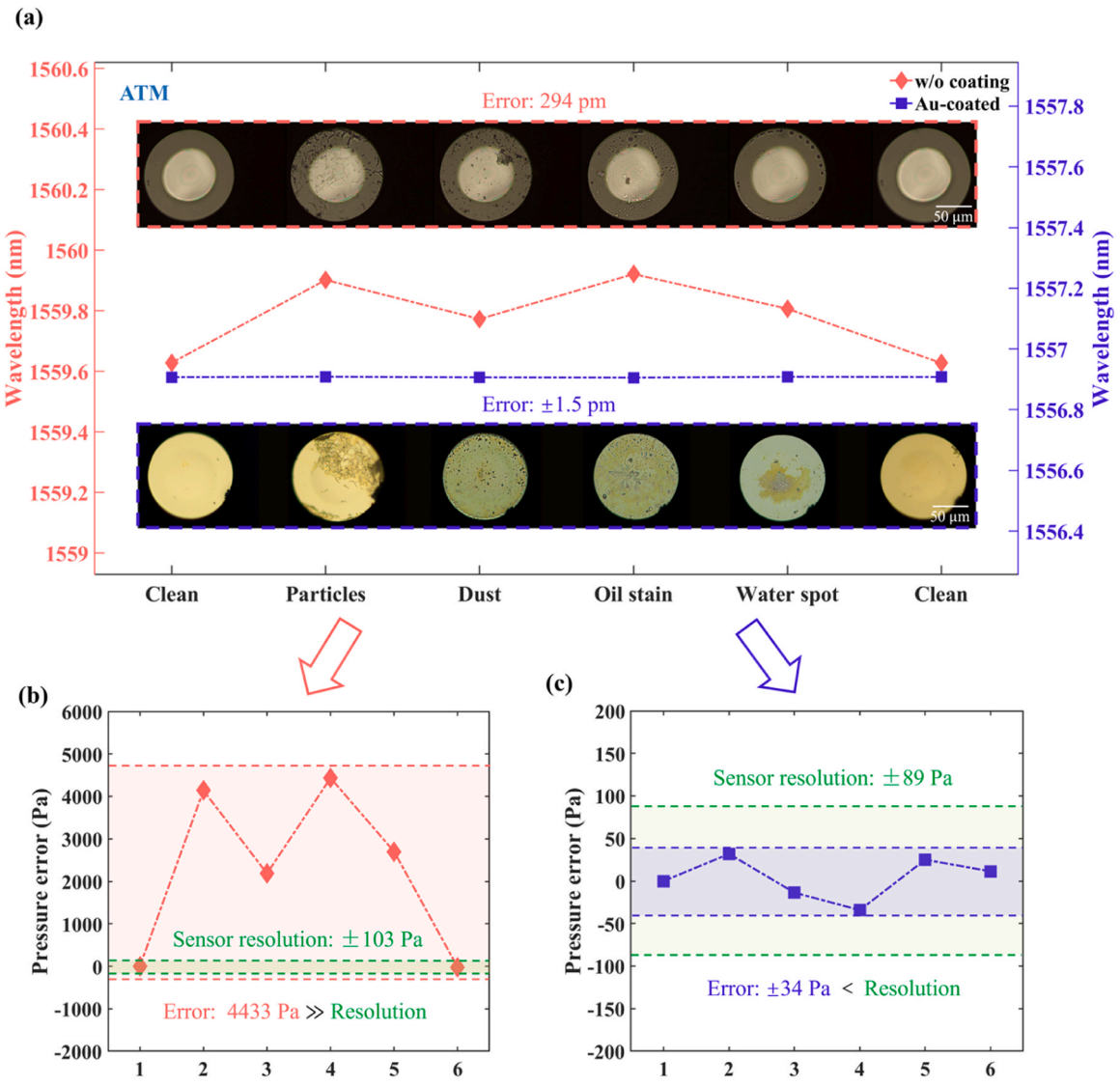

Fig. 4. Stain resistance test, (a) the wavelength shift of uncoated FP sensor and Au-coated FP sensor contaminated with different types of soiling under ATM and top views of the sensors under the microscope, (b) pressure measurement errors of the uncoated FP sensor caused by different types of soiling, (c) pressure measurement errors of the Au-coated FP sensor caused by different types of soiling.

where γ and E are Poisson's ratio and Young's modulus of the diaphragm, respectively, a is the effective radius, and h is the thickness of the quartz diaphragm. This work's diaphragm variation should take into account the more complex combined action of metal and quartz. A phase demodulation method was used for flow field measurements by fitting the measured spectra and calibrating the wavelength drift at different pressures in advance.

The FP sensor has been constructed in the following ways: first, as illustrated in Fig. 2(b) and (c), the SMF, hollow glass tube, and coreless optical fiber are welded together using a laser welding technique. Ideal quartz diaphragms were then produced by laser dicing and polishing, as shown in Fig. 2(d). Subsequently, the diaphragm is etched using buffered oxide etch (BOE). By precisely controlling parameters such as environmental temperature, solution concentration, and etching time, a diaphragm with a precise thickness can be obtained to enhance the sensitivity of the FP sensor. Ultimately, as illustrated in Fig. 2(e), a layer of gold with a thickness of 30 nm was applied by electron beam evaporation to the quartz diaphragm's cleaned surface in order to enhance the reflectivity of the FP outer surface, thereby reducing measurement errors caused by environmental pollution. Side and top views of the proposed fiber-optic FP sensor under an optical microscope are shown in Fig. 2(f).

3. Experimental results and discussion

The self-developed demodulation system consists of a tunable laser, a field programmable gate array (FPGA) control and acquisition module, and a photodetector (PD). The full-spectrum wavelength meets the needs of highly unsteady flow field measurements by scanning from 1527 nm to 1567 nm at a frequency of up to 30 kHz.

3.1. Characterization experiment of the FP sensor

Fig. 3(a) demonstrates the experimental setup for the calibration of the FP sensor integrated pressure probe. The optical pressure probe is sealed within a rubber conduit extending from the pressure generator. Data acquisition is realized by our self-developed demodulation system. The output interference spectrum is processed by fitting and peak-finding algorithms to obtain the drift value of the spectrum, which can be expressed as a function of the pressure. Fig. 3(b) and (c) illustrate the pressure response and the shift in the output interference spectra of our FP sensor in the range of 0~200 kPa, and the sensitivity is 43.90 pm/

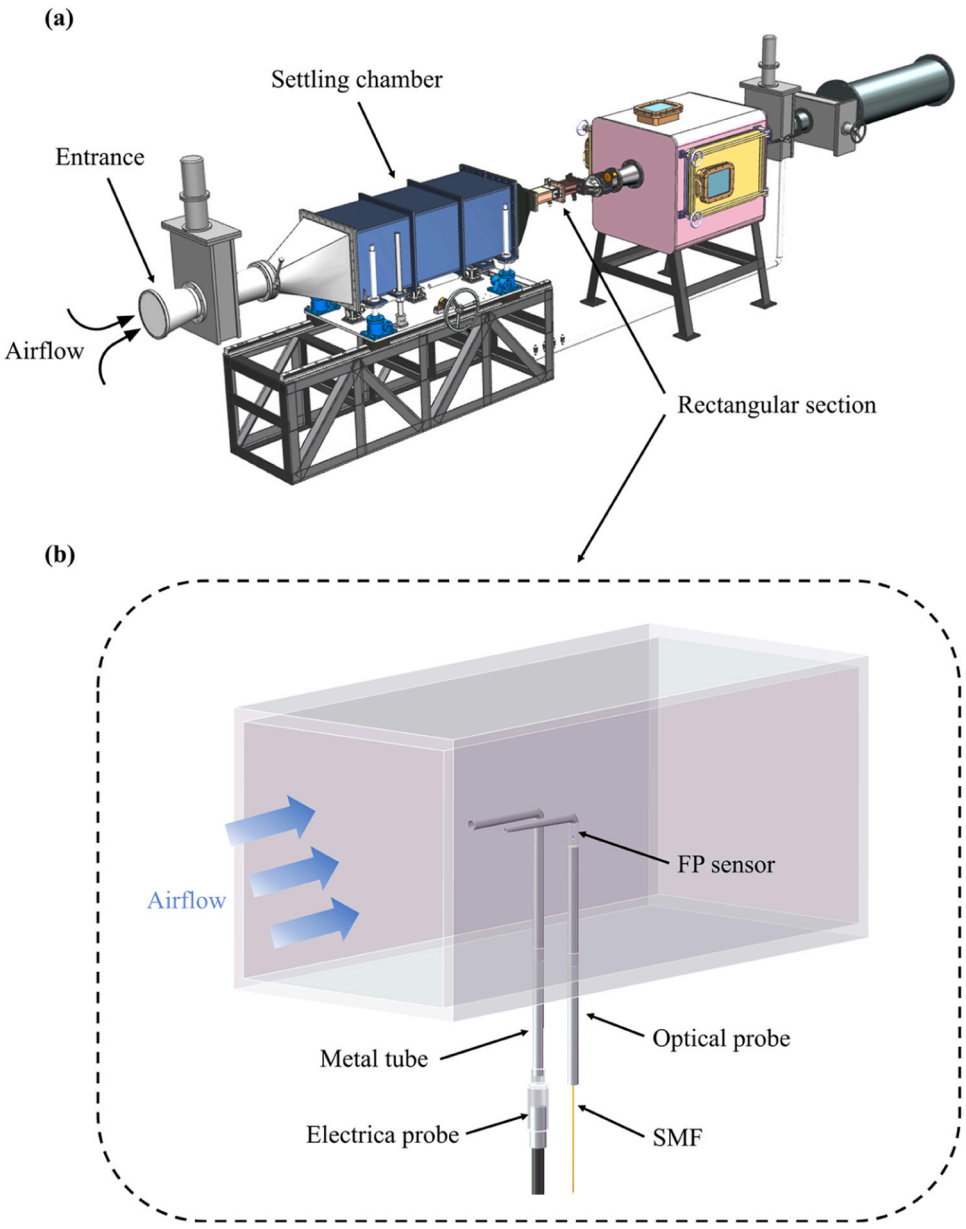

Fig. 5. Experimental setup, (a) the general arrangement of the test rig, (b) probe installation.

kPa. Our FP sensor maintains high linearity over a large measuring range, with a coefficient of determination (R^2) of 0.99, which is beneficial for practical measurements. The pressure resolution of the FP sensor is calculated by measuring the standard deviation (SD) of the measured wavelength. The measured wavelength is recorded at 5 kPa pressure for 6 s, as indicated in Fig. 3(d), with an SD of roughly 3.9 pm. The resolution of the FP sensor can be calculated as twice the SD (7.8 pm), and the pressure resolution of the FP sensor is about 178 Pa, which is 0.089 % of the full scale (F.S., 0~200 kPa). Subsequently, the temperature response characteristics of the FP sensor were investigated. As illustrated in Fig. 3(e), the FP sensor demonstrates a linear response to temperature variations within the range of 17 °C to 51 °C, with a sensitivity of 8.71 pm/°C, resulting in a temperature dependence of 0.198 kPa/°C. The temperature crosstalk primarily originates from the thermal expansion of the materials constituting the FP sensor. In applications with minimal temperature fluctuations, such as the constant-temperature wind tunnel experiments conducted in this study, this error can be considered negligible. For scenarios involving significant temperature variations, temperature compensation methods may be implemented, such as connecting an FBG fiber optic temperature sensor in series or employing a dual-FP sensor configuration [21–23].

In wind tunnel experiments, transient and drastic pressure changes can generate moisture, and high-speed airflow often carries dust particles, oil contaminants, etc. These harsh conditions restrict the use of most electrical sensors, which require non-corrosive, dry, and clean measurement environments. Contamination can also affect conventional FP sensors by altering the reflectivity of their diaphragms, leading to measurement errors. Experiments were conducted to investigate the effects of different contaminants on a quartz diaphragm FP sensor. Fig. 4 (a) demonstrates the spectral wavelength shift of the sensor under standard atmospheric pressure (ATM) when exposed to different contaminants, revealing a substantial shift of 294 pm. The derived pressure error reached 4433 Pa, far exceeding the sensor's resolution of ±103 Pa, as shown in Fig. 4(b). To protect the FP sensor integrated at the front end of the pressure probe from contamination, the proposed FP sensor was Au-coated. Comparison experiments were conducted to demonstrate the robustness of Au-coated FP sensor in dirty environments. As shown in Fig. 4(a) and (c), the spectral wavelength shift of the sensor

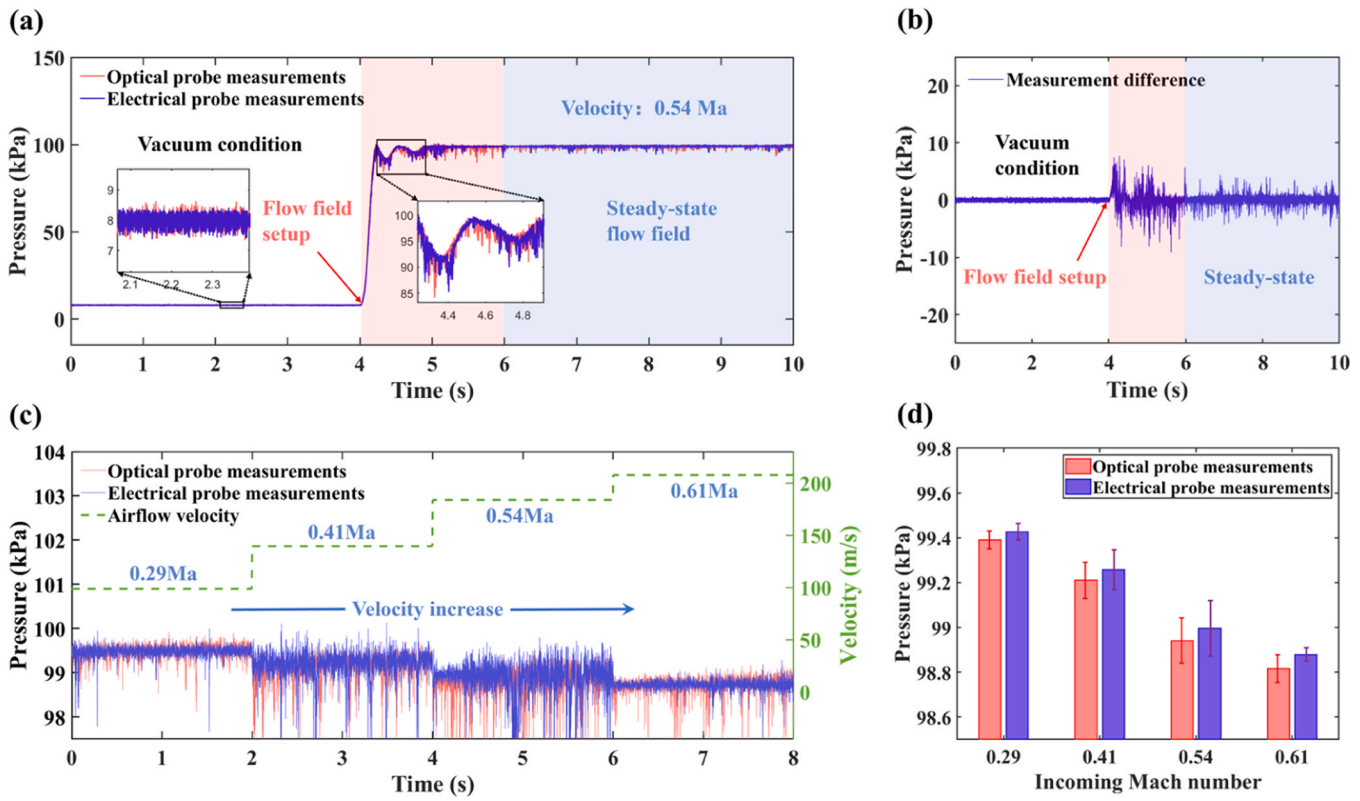

Fig. 6. Pressure measurements of airflow at velocities of 0.29–0.61 Mach in a wind tunnel, (a) responses of optical and electrical probes at incoming Mach numbers of 0.54 Ma, (b) measurement difference between optical and electrical probes at incoming Mach numbers of 0.54 Ma, (c) simultaneous measurement results of optical and electrical probes at incoming Mach numbers of 0.29 Ma, 0.41 Ma, 0.54 Ma, and 0.61 Ma, (d) comparison of optical and electrical probe measurements at incoming Mach numbers of 0.29 Ma, 0.41 Ma, 0.54 Ma, and 0.61 Ma.

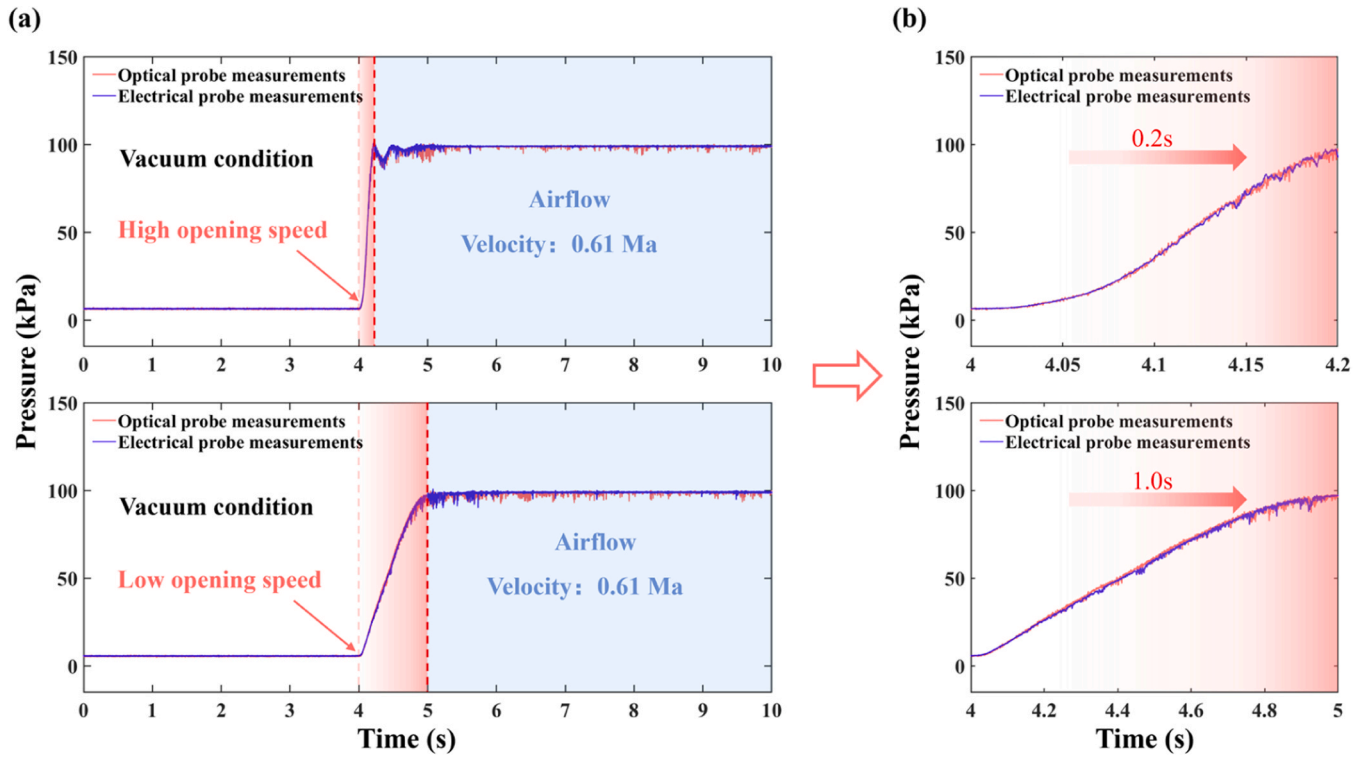

Fig. 7. Dynamic response characteristics of optical and electrical probes under varying valve opening speeds, (a) responses of optical and electrical probes under high and low valve opening speed at the incoming Mach number of 0.61 Ma, (b) result of Fig. 6(a) after stretching the time coordinate.

contaminated with different types of soiling was ±1.5 pm, which is two orders of magnitude smaller than that of FP sensor without coating, and the pressure measurement errors caused by contamination were ±34 Pa, equivalent to 0.017 % of the full-scale range (FS: 200 kPa). Notably, these contamination-induced errors remained within the sensor's resolution (±89 Pa), rendering their impact negligible. The Au coating applied to the external reflective surface of the FP cavity introduces a reflectivity mismatch between the two mirrors, leading to a partial reduction in interference fringe visibility. Nevertheless, this compromise is deemed acceptable when balanced against the measurement errors that would arise from surface contamination.

3.2. Pressure measurement in a wind tunnel

The experiments are conducted at the internal flow test rig. The available Mach number ranges from 0.2 to 0.7, and the test time for a single run is typically 60 s. The general arrangement of the test rig is shown in Fig. 5(a). A bellmouth is installed at the entrance and connected to the throttling device, which can regulate the incoming total pressure. A downstream settling chamber with two layers of honeycomb mesh, modeled after the smooth flow of cruising conditions, is located next to the throttling device. Following the settling chamber, the flow accelerates in a contraction section before entering a straight, rectangular section that is 300 mm long, 100 mm wide, and 50 mm high. As shown in Fig. 5(b), within this rectangular section, our optical pressure probe is co-located with a state-of-the-art piezo-resistive transducer (Shuangqiao CYG502) to facilitate concurrent measurements, ensuring a comparative analysis of the flow characteristics within the test environment. To minimize the contact area between the probe tip and the flow field, electrical probes require connection via a guide tube and a front-end probe during flow field measurements, whereas the proposed FP sensor, leveraging its compact size, can be directly integrated at the probe tip.

As illustrated in Fig. 6(a), the settling chamber is initially subjected to a vacuum to create a vacuum condition. Upon valve opening, the gas rushes into the chamber at high velocity. During the initial period of airflow introduction, the flow field remains unstable, resulting in fluctuations in the measured total pressure values. Subsequently, the flow field stabilizes over time. Fig. 6(b) illustrates the measurement difference between optical and electrical probes at incoming Mach numbers of 0.54 Ma. Under unsteady flow conditions, relatively large measurement discrepancies are observed between the two sensors, likely attributed to their positional variations inducing differential responses to the dynamic flow field. The rate of gas flow can be adjusted by modifying the degree to which the throttling device is opened. As shown in Fig. 6(c), the measurement results are presented at different incoming Mach numbers of 0.29 Ma, 0.41 Ma, 0.54 Ma, and 0.61 Ma, respectively. The optical pressure probe's measurement results are shown by the red lines, while the electrical pressure probe's measurement results are shown by the blue lines. It is evident that the two measures are consistent with one another. Fig. 6(d) compares the results with the measurements from the electrical probe and shows that they are essentially consistent. The high-speed wind tunnel's temperature fluctuations likely cause the slightly lower optical probe readings than electrical probe readings. Since the electrical sensor and probe were connected through a conduit, and the FP sensor was located near the probe's port, sensor positioning may also have an impact on this discrepancy. Additionally, the discrepancies in the calibration processes of the electrical and optical probes may also contribute to this systematic measurement error.

Gas can flow into the chamber at varying speeds by adjusting the valve opening speed. Fig. 7(a) and (b) show the response curves for two valve opening speeds at the incoming Mach number of 0.61 Ma, illustrating the dynamically changing measurements. Fig. 7(c) and (d) show the results after stretching the time coordinate, making it easier to see the transient pressure changes. In the graphs above, red and blue curves represent the test results of the optical and electrical probes, respectively. Our optical probes also appear to be in good agreement with the electrical probes. The airflow rate takes 0.2 and 1 s, respectively, to reach its maximum value for the two valve opening speeds.

Table 1
Comparison of the proposed optical probe to the Shuangqiao CYG502.

		Proposed optical probe	Shuangqiao CYG502
Dimension (diameter)	(mm)	0.5	2.1
Pressure range	(kPa)	0–200	0–100
Pressure resolution	(%)	0.09	0.25
Sampling rate	(kHz)	30	20
Pressure media		Most liquids or gases	Noncorrosive, dry, and clean gases

A comparison of the proposed optical probe to the Shuangqiao CYG502 piezo-resistive transducer is shown in Table 1. In addition to being competitive in size, accuracy, and measurement speed, the optical pressure probe can function well in corrosive environments, high temperatures, and high humidity levels. It is also resistant to electromagnetic interference.

4. Conclusion

A miniature aerodynamic pressure probe integrated with a fiber-optic FP sensor is demonstrated. Its packaging size is much smaller than a commercial electrical probe. The optical pressure probe shows a resolution of 0.089 % within a 0~200 kPa pressure range in a subsonic flow field (Mach: 0.29–0.61). The experimental results are in good agreement with those of the electrical probe, showing superior response and detection accuracy of the optical probe. Our findings may be helpful in studying highly unsteady flows, especially when it comes to studying the flow fields at high speeds and high spatial resolution. This will further the field of high-performance aircraft research. While future work will concentrate on improving the sensor design—for example, by adding temperature corrections—so that it can be used in more wind tunnel scenarios, realizing a dense distribution of probe points on the AIP is an important area of study for inlets, with the potential to uncover more hydrodynamic issues.

CRediT authorship contribution statement

Xi Chen: Conceptualization, Formal analysis, Investigation, Visualization, Writing – original draft. **Zhengkang Lin:** Investigation, Validation, Methodology, Writing – original draft. **Fen Xiong:** Resources, Investigation, Methodology. **Hexia Huang:** Supervision, Project administration, Writing – review & editing. **Ye Chen:** Supervision, Project administration, Writing – review & editing. **Huijun Tan:** Supervision, Project administration. **Fei Xu:** Supervision, Funding acquisition, Project administration, Writing – review & editing.

Declaration of Competing Interest

The authors declare that they have no known competing financial interests or personal relationships that could have appeared to influence the work reported in this paper.

Acknowledgements

This study was co-supported by the National Natural Science Foundation of China (61925502, 62135007, 62005118, 62035006, 12272177, and 12172175). The Research Fund of State Key Laboratory of Mechanics and Control of Mechanical Structures, Nos. MCMS-E-0522Y02.

Data availability

Data will be made available on request.

References

[1] J. Westerweel, et al., Particle image velocimetry for complex and turbulent flows, Annu. Rev. Fluid Mech. 45 (2013) 409–436.
[2] Q. Li, et al., Laser Doppler Velocimetry (LDV) measurements of airfoil surface flow on a Horizontal Axis Wind Turbine in boundary layer, Energy 183 (2019) 341–357.
[3] D. Telionis, , Recent Developments in Multi-Hole Probe (MHP) Technology, 2009.
[4] J.F. Brouckaert, Fast response aerodynamic probes for measurements in turbomachines, Proc. Inst. Mech. Eng. Part J. Power Energy 221 (2007) 811–813.
[5] F. Schettini, G. Di Rito, R. Galatolo, Smart air-data probe for fault-tolerant flow measurements, in: 2018 5th IEEE International Workshop on Metrology for AeroSpace (MetroAeroSpace), IEEE, Rome, 2018, pp. 602–607, https://doi.org/10.1109/MetroAeroSpace.2018.8453555.
[6] S.L. Stahl, D.V. Gaitonde, R.W. Powers, J.T. Spyropoulos, Modal analysis of serpentine diffuser distortion, in: AIAA AVIATION 2023 Forum, American Institute of Aeronautics and Astronautics, San Diego, CA, 2023, 10.2514/6.2023-3308.
[7] J. Crowder, et al., Airplane flow-field measurements, in: 1997 World Aviation Congress, American Institute of Aeronautics and Astronautics, Anaheim,CA,U.S.A., 1997, 10.2514/6.1997-5535.
[8] Y. Zhu, et al., Miniature fiber-optic pressure sensor, IEEE Photonics Technol. Lett. 17 (2005) 447–449.
[9] D. Donlagic, et al., All-fiber high-sensitivity pressure sensor with SiO2 diaphragm, Opt. Lett. 30 (2005) 2071–2073.
[10] S. Liu, et al., Nano silica diaphragm in-fiber cavity for gas pressure measurement, Sci. Rep. 7 (2017) 787.
[11] H. Zhang, et al., Miniature all-silica microbubble-based fiber optic Fabry-Perot pressure sensor with pressure leading-in tube, J. Sens. 2019 (2019) 1–7.
[12] J. Li, et al., Batch-producible all-silica fiber-optic Fabry–Perot pressure sensor for high-temperature applications up to 800 °C, Sens. Actuators A Phys. 334 (2022).
[13] H.B. Land, et al., Optical pressure measurement: using fiber optic transducers in hypersonic flight vehicles, IEEE Instrum. Meas. Mag. 7 (2004) 38–45.
[14] A. Cipullo, et al., Numerical study of a ferrule-top cantilever optical fiber sensor for wind-tunnel applications and comparison with experimental results, Sens. Actuators Phys. 178 (2012) 17–25.
[15] N.J. Lawson, et al., Development and application of optical fibre strain and pressure sensors for in-flight measurements, Meas. Sci. Technol. 27 (2016) 104001.
[16] F.M. Heckmeier, et al., Development of unsteady multi-hole pressure probes based on fiber-optic pressure sensors, Eng. Res. Express 1 (2019) 025023.
[17] Y. Liu, et al., Differential-pressure fiber-optic airflow sensor for wind tunnel testing, Opt. Express 28 (2020) 25101.
[18] S. Pevec, et al., Miniature fiber-optic pitot tube sensor, IEEE Sens. J. 20 (2020) 4732–4739.
[19] H. Zhou, et al., A MEMS-based fast-response miniature five-hole probe with optical pressure transducers, J. Microelectromech. Syst. 29 (2020) 960–965.
[20] Y. Liu, et al., Fiber-optic integrated aerodynamic three-hole vector probe for high-velocity flow field measurement, iScience 25 (2022) 104402.
[21] M. Li, et al., Optical MEMS pressure sensor based on Fabry-Perot interferometry, Opt. Express 14 (2006) 1497–1504.
[22] P. Jia, et al., Batch-producible MEMS fiber-optic Fabry–Perot pressure sensor for high-temperature application, Appl. Opt. 57 (2018) 6687–6692.
[23] X. Jiang, et al., Hybrid fiber optic sensor, based on the Fabry-Perot Interference, assisted with fluorescent material for the simultaneous measurement of temperature and pressure, Sensors 19 (2019) 1097.
[24] X. Wang, et al., All-silicon dual-cavity fiber-optic pressure sensor with ultralow pressure-temperature cross-sensitivity and wide working temperature range, Photon. Res. 9 (2021) 521–529.
[25] V. Bhatia, K.A. Murphy, R.O. Claus, T.A. Tran, J.A. Greene, Recent developments in optical-fiber-based extrinsic Fabry-Perot interferometric strain sensing technology, Smart Mater. Struct. 4 (1995) 246–251.
[26] Y. Chen, et al., Recent progress in MEMS fiber-optic Fabry–Perot pressure sensors, Sensors 24 (2024) 1079.
[27] A. Wang, et al., Self-calibrated interferometric-intensity-based optical fiber sensors, J. Light. Technol. 19 (2001) 1495–1501.
[28] J. Jia, et al., Dual-wavelength DC compensation technique for the demodulation of EFPI fiber sensors, IEEE Photonics Technol. Lett. 30 (2018) 1380–1383.
[29] J. Mei, X. Xiao, C. Yang, High-resolution and large dynamic range fiber extrinsic Fabry–Perot sensing by multi-extrema-tracing technique, Appl. Opt. 54 (2015) 3677.
[30] T. Liu, G.F. Fernando, A frequency division multiplexed low-finesse fiber optic Fabry–Perot sensor system for strain and displacement measurements, Rev. Sci. Instrum. 71 (2000) 1275–1278.
[31] H. Hassanieh, P. Indyk, D. Katabi, E. Price, Simple and practical algorithm for sparse fourier transform, in: Proceedings of the Twenty-Third Annual ACM-SIAM Symposium on Discrete Algorithms, Society for Industrial and Applied Mathematics, 2012, pp. 1183–1194, https://doi.org/10.1137/1.9781611973099.93.
[32] Z. Yu, Z. Tian, A. Wang, Simple interrogator for optical fiber-based white light Fabry–Perot interferometers, Opt. Lett. 42 (2017) 727.
[33] T. Liu, et al., Simultaneous measurement of pressure and temperature based on adjustable line scanning polarized low-coherence interferometry with compensation plate, IEEE Photonics J. 10 (2018) 1–9.
[34] Y. Zhou, et al., Application of machine learning in optical fiber sensors, Measurement 228 (2024) 114391.
[35] Y. Zhao, et al., Machine learning assisted fast demodulation of large dynamic range dual-parameter optical fiber sensors, IEEE Sens. J. 23 (2023) 31440–31446.

Xi Chen is currently pursuing the Ph.D. degree with the College of Engineering and Applied Sciences and Collaborative Innovation Center of Advanced Microstructures, Nanjing University, Nanjing, China. His main research interest includes fiber optic sensing and imaging.

Zhengkang Lin is currently pursuing the Ph.D. degree with the College of Energy and Power Engineering, Nanjing University of Aeronautics and Astronautics, Nanjing, China.

Fen Xiong is currently pursuing the Ph.D. degree with the College of Physics, MIIT Key Laboratory of Aerospace Information Materials and Physics, Nanjing University of Aeronautics and Astronautics, Nanjing, China.

Hexia Huang is currently an Associate Professor with the College of Energy and Power Engineering, Nanjing University of Aeronautics and Astronautics, Nanjing, China. His interests include radar-absorbing material fabrication for engine inlets, aero-stealth integrated design, aerodynamic inlet configuration, and advanced flow measurement techniques.

Ye Chen was born in Yanchen. He received the Bachelor degree in Electronic Science and Technology and the PhD degree in Optical Engineering from Nanjing University, Nanjing, China in 2008 and 2015, respectively. His main research interest includes optical devices and wearable devices.

Huijun Tan is currently a Professor with the College of Energy and Power Engineering, Nanjing University of Aeronautics and Astronautics, Nanjing, China. His long-term research focuses on engine inlet technologies, inlet/aircraft integration, and high-speed internal flow aerodynamics.

Fei Xu (Senior Member, IEEE) received the Ph.D. degree from the Optoelectronics Research Centre, University of Southampton, Southampton, U.K., in 2008. He is currently a Professor with the College of Engineering and Applied Sciences and Collaborative Innovation Center of Advanced Microstructures, Nanjing University, Nanjing, China. His interests include fibre optic sensing and lasers, wearable medical monitoring, and medical imaging.